# Strong proximal earthquakes revealed by cosmogenic ³He dating of prehistoric rockfalls, Christchurch, New Zealand

Benjamin H. Mackey and Mark C. Quigley
Department of Geological Sciences, University of Canterbury, Private Bag 4800, Christchurch 8140, New Zealand

## ABSTRACT

The 2011 rupture of previously undetected blind faults beneath Christchurch, New Zealand, in moment magnitude ($M_w$) 6.2 and 6.0 earthquakes triggered major rockfalls that caused fatalities and infrastructure damage. Here we use field, geospatial, seismologic, numerical modeling, and cosmogenic ³He data to provide first evidence for prehistoric rockfall ca. 8–6 ka, and a possible preceding event ca. 14–13 ka, at a site where extensive rockfall occurred in the Christchurch earthquakes. The long (~7 ± 1 k.y.) time intervals between successive rockfall events and the high peak ground velocity thresholds required for rockfall initiation at this site (~20–30 cm/s) preclude earthquakes from major identified seismic sources, including the plate boundary Alpine fault, as likely rockfall triggering sources. Rockfalls were probably triggered by strong paleoearthquakes sourced from active faults proximal (i.e., <10–20 km) to Christchurch, including the sources of the 2011 Christchurch earthquakes and/or other currently unidentified faults. Given the inherent incompleteness of seismic source catalogues and challenges in obtaining earthquake chronologies for blind faults, high scientific priority should be given to the search for, and analysis of, geologic records of strong earthquake shaking near populated areas.

## INTRODUCTION

Active faults capable of generating highly damaging earthquakes may not cause surface rupture (i.e., blind faults), or may cause surface ruptures that evade detection due to subsequent burial or erosion by surface processes. Fault populations and earthquake frequency-magnitude distributions adhere to power laws (Main, 1996), implying that faults too small to cause surface rupture but large enough to cause strong ground shaking densely populate continental crust. Blind faults are underrepresented relative to larger, surface-rupturing faults in paleo-earthquake catalogues (Nicol et al., 2012). Recent earthquakes on previously unidentified and/or blind faults proximal to densely populated areas have caused catastrophic loss of life and infrastructure damage (Talebian et al., 2004; Calais et al., 2010; Beavan et al., 2012). At least 12 previously unknown faults ruptured in a series of moment magnitude ($M_w$) 5.9–7.1 earthquakes (Beavan et al., 2012) near Christchurch, New Zealand, in 2010 and 2011 (Fig. 1) (termed the Canterbury earthquake sequence). The 22 February 2011 $M_w$ 6.2 Christchurch earthquake (herein termed Christchurch I earthquake) resulted in 185 fatalities, and the Canterbury earthquake sequence caused more than US $30 billion of cumulative damage. Blind faults have been identified beneath other major population centers (Shaw and Shearer, 1999); however, the timing and frequency of paleo-earthquakes and likely patterns of coseismic shaking are challenging to quantify due to an inability to conduct direct investigations of these faults at the surface. Geological features that enable estimation of earthquake strong ground motions independent of fault source data are thus valuable for seismic hazard analyses (Brune, 1996).

A major hazard accompanying earthquake shaking in areas of steep topography is the detachment of rocks from bedrock outcrops that subsequently slide, roll, or bounce downslope (i.e., rockfalls). Five fatalities and significant infrastructural damage during the Christchurch I earthquake resulted from coseismic rockfall and cliff collapse (Bradley, 2013; Massey et al., 2014). Major rockfall also occurred in an $M_w$ 6.0 earthquake on 13 June 2011 (termed the Christchurch II-b earthquake) (Fig. 1). Here we use the emplacement time of prehistoric rockfall to constrain the temporal
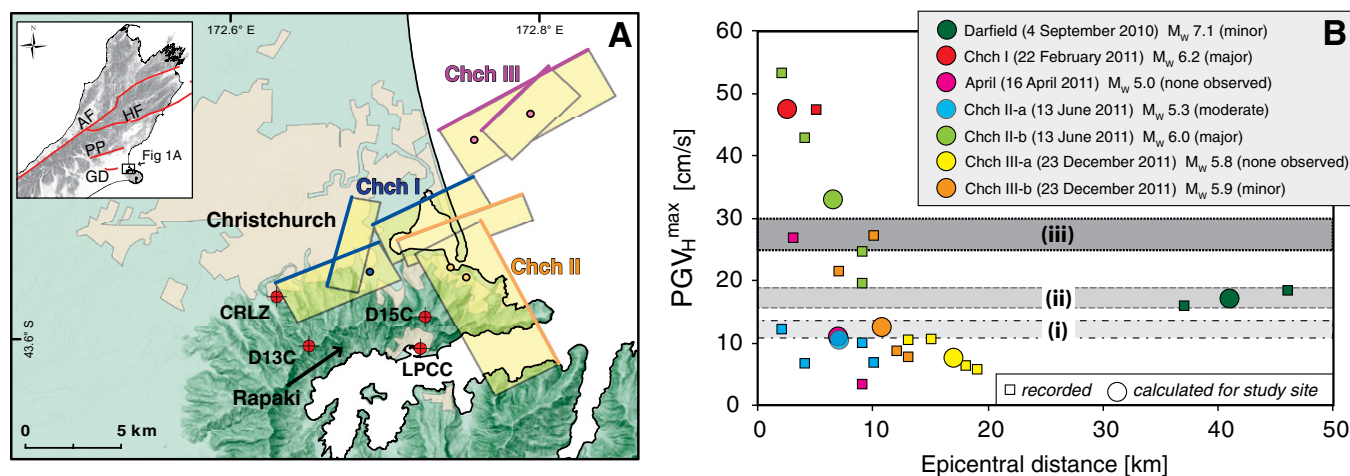


Figure 1. A: Christchurch, New Zealand, area showing location of Rapaki study site and blind fault sources (circles represent epicenters; shaded box is the fault plane; thick line shows surface projection of top of fault) from major 2011 earthquakes (Beavan et al., 2012). Chch I, II, and III are Christchurch earthquakes (see text). Seismic stations: LPCC—Lyttelton Port Company, D15C—Summit Road, D13C—Sign of the Kiwi, CRLZ—Canterbury Ring Laser. Inset shows northern South Island, with Alpine fault (AF), Hope fault (HF), Porters Pass fault (PP), and Greendale fault (GD) (the 2010 Darfield earthquake rupture). B: Processed instrumental maximum horizontal peak ground velocity ($PGV_H^{max}$) values for closest strong ground motion stations to the study site and estimated $PGV_H^{max}$ at the rockfall source cliff plotted against epicentral distance for the strongest earthquakes (i.e., highest recorded PGVs) between A.D. 2010 and 2011 for which occurrence or nonoccurrence of rockfall is known. $M_w$—moment magnitude. Rockfall $PGV_H^{max}$ triggering thresholds i–iii are described in text.

*E-mail: ben.mackey@canterbury.ac.nz.

distribution and likely sources of past strong ground shaking analogous to that of the Christchurch I and II-b earthquakes.

The measurement of cosmogenic nuclide concentrations in minerals exposed at or near Earth's surface has been used to estimate the age of paleorockfalls over $10^3$ to $10^4$ yr time scales (e.g., Matmon et al., 2005; Cordes et al., 2013; Rinat et al., 2014). This study is the first we know of to date paleorockfalls using cosmogenic $^3$He, a nuclide produced and retained in a variety of minerals, including clinopyroxene (augite) (Gosse and Phillips, 2001). The use of $^3$He concentrations to determine a boulder surface exposure age requires (1) isolating cosmogenic $^3$He from other potential sources of $^3$He (Lal, 1987), (2) consideration of possible pre-rockfall exposure history and possible inherited cosmogenic $^3$He concentrations in the sampled surface, and (3) consideration of possible complex post-rockfall exposure histories, including boulder mobility and/or burial and re-exhumation. Resolving these potential complications requires selective field sampling based on geologic and geomorphic criteria and careful interpretation of $^3$He concentrations for a population of boulder ages (see the GSA Data Repository[1]).

Mass movements, including landslides and rockfalls, have a range of potential triggers including earthquake shaking, intense or prolonged precipitation events, temperature fluctuations, fires, floral and faunal activity, groundwater changes, anthropogenic activity, and residual weathering (e.g., Tatard et al., 2010). The attribution of paleorockfalls to seismic events thus requires careful consideration of other feasible triggering mechanisms, including their probable behavior in time and space, and likely influences on rockfall boulder age populations.

## MODERN ROCKFALL AND PEAK GROUND VELOCITY THRESHOLDS AT RAPAKI

The Rapaki study site is located in the Port Hills of southern Christchurch (Figs. 1 and 2). The site consists of (1) steep to subvertical bedrock cliffs composed of stratified basaltic lava and indurated pyroclastic flow deposits, (2) a ~23° grassy slope composed of windblown sediment deposits (loess), overlying rockfall boulders, and colluvium, and (3) the village of Rapaki at the base of the slope. More than 650 individual boulders ranging in diameter from <15 cm to >3 m were dislodged from an ~60-m-tall and ~300-m-long source cliff in the Christchurch I and II-b earthquakes (Fig. 2). Boulders traveled distances of as much as 750 m downslope; some caused significant property damage (Fig. 2C).

A network of seismometers recorded ground motions during the Canterbury earthquake sequence (Table DR1 in the Data Repository). Because the fracture energy required to induce rockfall is directly proportional to peak ground velocity (PGV) (Andrews et al., 2007; Rathje et al., 2013), we use this measure (as opposed to other strong ground motion measures such as peak ground acceleration) to characterize rockfall-generating ground motions. A maximum horizontal PGV ($PGV_H^{max}$) of 47.5 cm/s was recorded during the Christchurch I earthquake at the seismometer closest to the study site (station LPCC; Fig. 1B; Table DR2). $PGV_H^{max}$ values at the closest seismometers during the Christchurch II-b earthquake were 43 cm/s (station LPCC), 53.4 cm/s (station D15C), and 24.8 cm/s (station D13C). Moderate (<10% of total observed) rockfall was observed in the $M_w$ 5.3 Christchurch II-a earthquake; the closest seismometers yielded $PGV_H^{max}$ of 7–12 cm/s. A few isolated rocks (<1% of total observed) were detached from the study site cliff in the 4 September 2010 $M_w$ 7.1 Darfield earthquake (LPCC $PGV_H^{max}$ = 18.5 cm/s; CRLZ $PGV_H^{max}$ = 16.1 cm/s) and 23 December 2011 $M_w$ 5.9 Christchurch III-b earthquake (LPCC $PGV_H^{max}$ = 27.3 cm/s; D15C $PGV_H^{max}$ = 21.5 cm/s). Rockfall did not occur at the site (but may have occurred elsewhere) in any other earthquakes during the Canterbury earthquake sequence for which there are observational accounts from local residents (e.g., 16 April 2011, $M_w$ 5.0; 23 December 2011, $M_w$ 5.8, Christchurch III-a; Fig. 1B).

We estimated $PGV_H^{max}$ at the source cliff for the strongest earthquakes using linear interpolation between the most proximally recorded PGVs (Fig. 1C). On the basis of rockfall observations and $PGV_H^{max}$ calculations, we propose a rockfall triggering threshold of $PGV_H^{max}$ = 12 ± 1 cm/s for the localized detachment of susceptible rocks in a previously fractured rock mass (minor to moderate $PGV_H^{max}$ rockfall threshold; i in Fig. 1B), $PGV_H^{max}$ = 17 ± 2 cm/s for localized rock fracture and rockfall in an intact rock mass (ii in Fig. 1B; e.g., the Darfield earthquake), and $PGV_H^{max}$ ≥ 25–30 cm/s for extensive rockfall and rock mass fracturing (iii in Fig. 1B; e.g., the
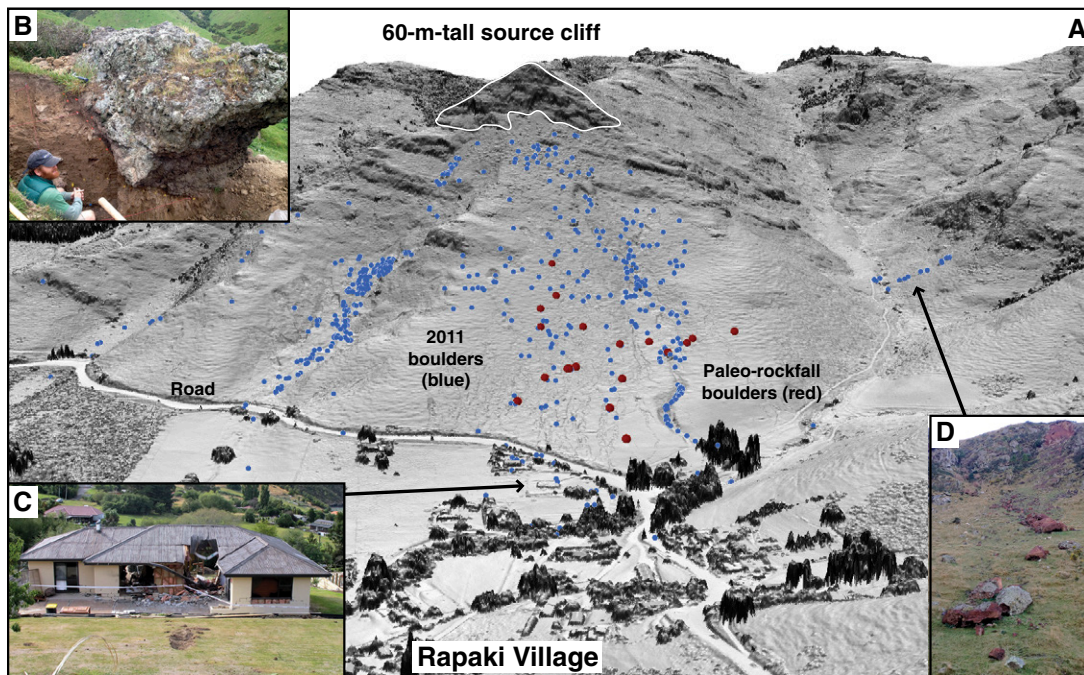


Figure 2. A: West-looking oblique lidar digital elevation map of slopes above Rapaki Bay, New Zealand, study site showing location of rockfall boulders displaced in 2011 Christchurch earthquakes (blue). Red dots indicate paleorockfall boulders sampled in this study. B: Partial excavation around paleorockfall boulder (Rap15). C: House damaged by rockfall in February 2011; impact crater is in foreground. House location is shown by arrow in A (photo courtesy of D. Barrell, GNS Science). D: Rockfall deposit in side valley, showing variability in boulder orientation on emplacement. Approximately half of the 2011 boulders landed with the fresh face oriented upright (Data Repository; see footnote 1).

Christchurch I earthquake). Variations in geology, elevation, and topography among seismometer sites contribute uncertainty to $PGV_H^{max}$ estimates.

## [3]He DATING AND SEISMIC ORIGIN OF PALEOROCKFALL

Hundreds of paleorockfall boulders with similar size and depositional extent to the modern boulders were identified at the study site (Fig. 2A). Paleorockfall boulders were distinguished from modern boulders because they are partially embedded in hillslope colluvium and are visible in pre–Canterbury earthquake sequence imagery. They have high degrees of surface roughness due to differential weathering of embedded basaltic blocks from the host matrix, and are extensively covered in lichen (Fig. 2B), indicating that they were emplaced long before European settlement in the 1850s. Paleorockfall boulders overlie (and thus were emplaced after) loess that likely accumulated on the slope during the 17−13 ka termination of the Last Glacial Maximum.

We collected samples for cosmogenic dating from the top surfaces of 19 of 25 accessible large (≥1.5 m diameter) paleorockfall boulders. Deeply shielded samples were obtained to quantify [3]He inherited from mantle and nucleogenic sources (see the Data Repository). Boulder undersides ($n = 6$) were sampled to assess possible inherited cosmogenic [3]He accrued while a boulder was in place on the cliff prior to detachment and postdepositional boulder mobility. The presence of thick colluvial wedges accumulated upslope of sampled boulders (Fig. 2B) and the absence of remobilization during the Canterbury earthquake sequence imply that boulders remained fixed in stable positions following deposition.

Augite [3]He concentrations and apparent exposure ages are presented in Tables DR3 and DR4 and in Figure 3. Prehistoric rockfall boulders have apparent surface exposure ages ranging from 6 to 70 ka; most ages are between 6 and 20 ka (Fig. 3A; Table DR4). [3]He concentrations obtained from the undersides of 4 of the younger 8–6 ka boulders (Table DR4) are well above background (cosmogenic shielded) levels, indicating boulder emplacement with faces formerly exposed on the source cliff now on the boulder underside, and formerly shielded faces now on the top. No surface exposure ages of 6 ka or younger were obtained, and we interpret this to reflect the time (7 ± 1 ka) of the most recent paleorockfall event. Another age cluster centered at 13 ± 2 ka may indicate the timing of a prior rockfall event or reflect [3]He inheritance in boulders emplaced ca. 7 ± 1 ka. Given the depositional age of the underlying loess, boulder exposure ages progressively older than ca. 13 ka are likely to indicate predetachment [3]He inheritance; boulders deposited on the hillslope before ca. 17–13 ka are likely to be buried beneath loess and colluvium.

To compare the measured distribution of rockfall ages to other simple rockfall-generating scenarios, we generated synthetic curves of the relative probability of a population boulder ages (Fig. 3B). We seeded a source population of rockfall boulders with randomized pre-rockfall [3]He concentrations equivalent to exposure ages ranging from 0 to 70 ka, the oldest measured bedrock exposure age. In a rockfall event, we drew boulders from this distribution, which were replaced with zero age boulders. We assumed cubic boulder morphologies, as evidenced from field observations. We assigned 0.17 probability that the postdepositional boulder top surface would be equivalent to the predetachment exposure age, and a 0.17 probability that the postdepositional boulder surface would be a fully shielded detachment surface, equating to zero age at emplacement. The remaining boulders have 0.66 probability they will be deposited on their side, with a partially shielded top surface (Fig. DR2). Partial shielding was calculated by modifying the external (cliff face) age of the boulder with a function to simulate the exponential decay of cosmogenic production into rock. We modeled three distinct rockfall production scenarios: (1) rockfall-generating events every 500 yr from 20 ka to present, (2) rockfall-generating events every 7 k.y. (14 ka, 7 ka), and (3) one rockfall-generating event at 7 ka (Fig. 3B).

In comparing modeled rockfall age distributions, scenario 1 is implausible given the observed age distributions and lack of post–6 ka
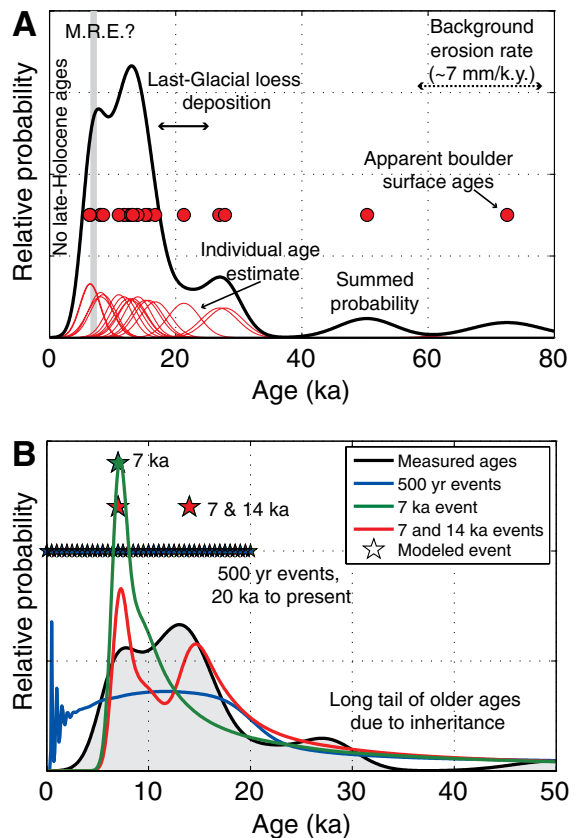
Figure 3. A: Apparent ages of boulder upper surfaces derived from cosmogenic [3]He exposure dating. Individual ages (indicated as Gaussian probability distribution functions) are shown as thin red lines, and summed probability of all ages is in black. Red dots denote individual central age estimates along an arbitrary y value to aid visualization. Gray band is probable most recent event (M.R.E.) at 7 ± 1 ka. B: Modeled age distribution probabilities for three rockfall scenarios and the measured age distribution shown in A (gray shading). The observed age pattern is best fit by modeled rockfall events ca. 7 and 14 ka. Stars indicate timing of modeled earthquakes for each scenario.

ages. The best fit between modeled and actual age distributions is scenario 2, although scenario 3 cannot be dismissed given the uncertainties in pre-rockfall inherited cosmogenic [3]He. The resolution of this dating technique does not allow us to dismiss the possibility of multiple rockfall events in temporally clustered paleo-earthquakes (i.e., <1−10[3] yr apart) analogous to Canterbury earthquake sequence.

We interpret the absence of boulder exposure ages younger than 7 ± 1 ka to indicate that no major rockfalls occurred at this site between that time and the 2011 Christchurch I earthquake. This conclusion is supported by regional geologic evidence for a near absence of pre–Canterbury earthquake sequence talus or rockfall debris at the base of nearby abandoned seacliffs cut during the mid-Holocene highstand (ca. 6–7 ka) (Brown et al., 1988). The 7 k.y. rockfall hiatus prior to the 2010–2011 Canterbury earthquake sequence spans a time period encompassing major changes in climate, extreme weather, extensive devegetation since the 17th century, and continued residual weathering of the source cliff. The highly consolidated, coarsely jointed nature of the basaltic rock mass in the study area appears to make it less susceptible to nonseismic rockfall triggering, particularly compared to other lithologies, such as the highly fractured greywacke of New Zealand's Southern Alps (Tatard et al., 2010).

The hiatus includes many large earthquakes on the largest seismic sources in the region (Stirling et al., 2012), including the Alpine fault ($M_w$

7.6–8.2, every ~300–400 yr) (Berryman et al., 2012) and Porters Pass fault ($M_w$ 7.1–7.5, every ~1500–2000 yr) (Howard et al., 2005) (Fig. 1). This suggests that no late Holocene earthquakes sourced from these faults caused rockfall at the study site. Numerical modeling using ground motion prediction equations (Bradley, 2013) and maximum $M_w$ estimates suggests that no active fault currently identified in the New Zealand seismic hazard model (Stirling et al., 2012; Litchfield et al., 2013) generates median (50th percentile) horizontal PGVs at the base of the study site above 10 cm/s (Fig. DR3).

PGV estimates from known sources are <13 cm/s even when considering possible PGV amplification of as much as 60% at the study site due to topographic effects and site conditions (Khajavi et al., 2012). Strong earthquake shaking above the estimated PGV threshold generated by earthquakes on proximal faults thus provides the most likely explanation for the origin of the Rapaki paleorockfalls. Although the fractured current state of parts of the source cliff does not negate the possibility of future isolated rockfalls occurring at PGVs less than that of the proposed threshold (or in the absence of earthquake shaking), the lack of significant rockfall in the Christchurch III-b earthquake at PGVs higher than predicted median PGV for these regional seismic sources suggests that total volumes would be small and limited to particularly susceptible areas of the rock mass under these conditions.

A reasonable conclusion is that the ca. 7 ka (and possibly the 14–13 ka) paleorockfalls provide a tentative, shaking-based recurrence interval for earthquakes on the faults responsible for the Christchurch I and II-b earthquakes, although testing this hypothesis will require further careful study of earthquake shaking proxies throughout the region. The possibility that other unidentified faults in the area triggered rockfalls and thus pose a major seismic hazard to Christchurch cannot be dismissed; based on crustal attenuation relationships and our proposed PGV thresholds, the maximum distances of the closest rupture tips to the study site are likely to be <10 km for $M_w$ 6.0 earthquakes and <20 km for $M_w$ 7.0 earthquakes.

## IMPLICATIONS

As evident from this study and others (e.g., Evans and Hungr, 1993), paleorockfall deposits are clear evidence of the most likely locations of future rockfall. In this instance, modern rockfalls were triggered by rare, strong ground motions sourced from earthquakes on blind faults proximal to a major urban center that evaded detection until the Canterbury earthquake sequence. Given the challenges in obtaining earthquake chronologies, $M_w$ potentials, and expected shaking intensities associated with blind fault ruptures, particularly in the absence of historical seismicity, geologic proxies for past strong ground motion are valuable to predict the impacts of future strong earthquakes regardless of their seismic source. This should be particularly prioritized for urban settings, where comparably moderate (i.e., $M_w$ 6–6.5) proximal earthquakes on blind and/or unidentified faults may be the largest shaking hazard.

## REFERENCES CITED

Andrews, D.J., Hanks, T.C., and Whitney, J.W., 2007, Physical limits on ground motion at Yucca Mountain: Seismological Society of America Bulletin, v. 97, p. 1771–1792, doi:10.1785/0120070014.

Beavan, J., Motagh, M., Fielding, E.J., Donnelly, N., and Collett, D., 2012, Fault slip models of the 2010–2011 Canterbury, New Zealand, earthquakes from geodetic data and observations of postseismic ground deformation: New Zealand Journal of Geology and Geophysics, v. 55, p. 207–221, doi:10.1080/00288306.2012.697472.

Berryman, K.R., Cochran, U.A., Clark, K.J., Biasi, G.P., Langridge, R.M., and Villamor, P., 2012, Major earthquakes occur regularly on an isolated plate boundary fault: Science, v. 336, p. 1690–1693, doi:10.1126/science.1218959.

Bradley, B.A., 2013, A New Zealand–specific pseudospectral acceleration ground-motion prediction equation for active shallow crustal earthquakes based on foreign models: Seismological Society of America Bulletin, v. 103, p. 1801–1822, doi:10.1785/0120120021.

Brown, L.J., Wilson, D.D., Moar, N.T., and Mildenhall, D.C., 1988, Stratigraphy of the late Quaternary deposits of the northern Canterbury Plains, New Zealand: New Zealand Journal of Geology and Geophysics, v. 31, p. 305–335, doi:10.1080/00288306.1988.10417779.

Brune, J.N., 1996, Precariously balanced rocks and ground-motion maps for southern California: Seismological Society of America Bulletin, v. 86, p. 43–54.

Calais, E., Freed, A., Mattioli, G., Amelung, F., Jonsson, S., Jansma, P., Hong, S.-H., Dixon, T., Prepetit, C., and Momplaisir, R., 2010, Transpressional rupture of an unmapped fault during the 2010 Haiti earthquake: Nature Geoscience, v. 3, p. 794–799, doi:10.1038/ngeo992.

Cordes, S.E., Stock, G.M., Schwab, B.E., and Glazner, A.F., 2013, Supporting evidence for a 9.6 ± 1 ka rock fall originating from Glacier Point in Yosemite Valley, California: Environmental & Engineering Geoscience, v. 19, p. 345–361, doi:10.2113/gseegeosci.19.4.345.

Evans, S.G., and Hungr, O., 1993, The assessment of rockfall hazard at the base of talus slopes: Canadian Geotechnical Journal, v. 30, p. 620–636, doi:10.1139/t93-054.

Gosse, J.C., and Phillips, F.M., 2001, Terrestrial in situ cosmogenic nuclides: Theory and application: Quaternary Science Reviews, v. 20, p. 1475–1560, doi:10.1016/S0277-3791(00)00171-2.

Howard, M., Nicol, A., Campbell, J., and Pettinga, J.R., 2005, Holocene paleoearthquakes on the strike-slip Porters Pass fault, Canterbury, New Zealand: New Zealand Journal of Geology and Geophysics, v. 48, p. 59–74, doi:10.1080/00288306.2005.9515098.

Khajavi, N., Quigley, M., McColl, S.T., and Rezanejad, A., 2012, Seismically induced boulder displacement in the Port Hills, New Zealand during the 2010 Darfield (Canterbury) earthquake: New Zealand Journal of Geology and Geophysics, v. 55, p. 271–278, doi:10.1080/00288306.2012.698627.

Lal, D., 1987, Production of He-3 in terrestrial rocks: Chemical Geology, v. 66, p. 89–98.

Litchfield, N.J., et al., 2013, A model of active faulting in New Zealand: New Zealand Journal of Geology and Geophysics, v. 57, p. 32–56, doi:10.1080/00288306.2013.854256.

Main, I., 1996, Statistical physics, seismogenesis, and seismic hazard: Reviews of Geophysics, v. 34, p. 433–462, doi:10.1029/96rg02808.

Massey, C.I., et al., 2014, Determining rockfall risk in Christchurch using rockfalls triggered by the 2010–2011 Canterbury earthquake sequence, New Zealand: Earthquake Spectra, v. 30, p. 155–181, doi:10.1193/021413EQS026M.

Matmon, A., Shaked, Y., Porat, N., Enzel, Y., Finkel, R., Lifton, N., Boaretto, E., and Agnon, A., 2005, Landscape development in an hyperarid sandstone environment along the margins of the Dead Sea fault: Implications from dated rock falls: Earth and Planetary Science Letters, v. 240, p. 803–817, doi:10.1016/j.epsl.2005.06.059.

Nicol, A., Robinson, R., Van Dissen, R., and Harvison, A., 2012, Variability of single event slip and recurrence intervals for large magnitude paleoearthquakes on New Zealand's active faults: GNS Science Report 2012/41, 57 p.

Rathje, E., Wang, Y., Stafford, P., Antonakos, G., and Saygili, G., 2013, Probabilistic assessment of the seismic performance of earth slopes: Bulletin of Earthquake Engineering, v. 12, p. 1071–1090, doi:10.1007/s10518-013-9485-9.

Rinat, Y., Matmon, A., Arnold, M., Aumaître, G., Bourlès, D., Keddadouche, K., Porat, N., Morin, E., and Finkel, R.C., 2014, Holocene rockfalls in the southern Negev Desert, Israel and their relation to Dead Sea fault earthquakes: Quaternary Research, v. 81, p. 260–273, doi:10.1016/j.yqres.2013.12.008.

Shaw, J.H., and Shearer, P.M., 1999, An elusive blind-thrust fault beneath metropolitan Los Angeles: Science, v. 283, p. 1516–1518, doi:10.1126/science.283.5407.1516.

Stirling, M., et al., 2012, National seismic hazard model for New Zealand: 2010 update: Seismological Society of America Bulletin, v. 102, p. 1514–1542, doi:10.1785/0120110170.

Talebian, M., et al., 2004, The 2003 Bam (Iran) earthquake: Rupture of a blind strike-slip fault: Geophysical Research Letters, v. 31, L11611, doi:10.1029/2004GL020058.

Tatard, L., Grasso, J.R., Helmstetter, A., and Garambois, S., 2010, Characterization and comparison of landslide triggering in different tectonic and climatic settings: Journal of Geophysical Research, v. 115, F04040, doi:10.1029/2009jf001624.